On Force-free Eigenstates for Ball Lightning

Geert C. Dijkhuis, Convectron N.V., Rotterdam, The Netherlands

Abstract. For ball lightning and bosonic plasmas we derive force-free solutions in quaternion form. The quaternion matrix of electromagnetic potentials enforces zero magnetic field by regularity rules. St. Elmo's fire on windshields caused a 2006 ball lightning event inside a small jet plane. We model it as elementary Bessel function in quaternion form. Our 3D solution plots scalar and vector potentials in the formation phase of this plasma ball.

Linked streamers modeling ball lightning share field topology with Bose-Einstein condensate of ultra-cold atoms trapped by lasers [1,2]. Flux knots found in thermonuclear fusion plasmas inspired Ranada's magnetohydrodynamic model of ball lightning [2]. His formulas for field, current and energy ensure stability by conservation of helicity. Threading cool ambient plasma, hot streamers with 0,05-0,20 mm width and 2-8 m length radiate like laboratory plasma torches [2]. Initial magnetic field values 1-3 T suffice for lifetimes 3-22 s, in line with global data for ball lightning [3]. For laboratory tests Ranada suggests two transverse discharges with electrodes in rapid rotation.

A US team created similar linked-field textures in tenuous clouds of Rubidium atoms [1]. External magnetic fields control precession of atomic spins forming skyrmion textures in their test facility. Figure 1D shows magnetic field topology linking each loop just once with all other loops as in the elementary Hopf fibration. The topology of helical electric field lines in Figure 1E shows four junctions on the polar axis, tiling concentric spheres with helicity reversal in between. Thus laser-trapped ultra-cold quantum spins copy flux knots tied in ultra-hot fusion plasmas confined by magnetic fields.

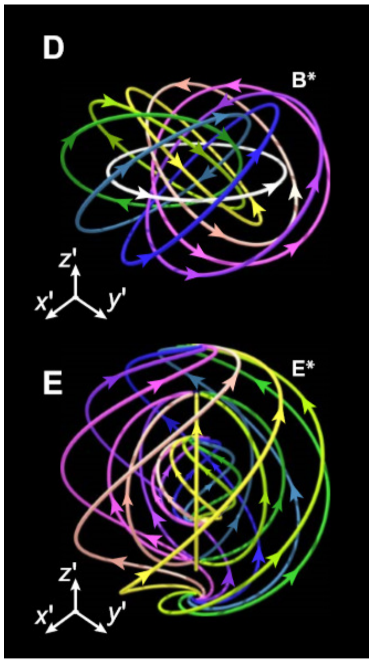

Figure 1. Skyrmion state links magnetic loops in (D) and twists electric field lines in (E) [1].

In refs. 1 and 2 spherical Bessel function j_0 scales the field solutions. The mathematical properties of j_0, its higher orders j_n, their modified forms y_n and extension into complex planes are readily available [4].

Earlier electric profiles treat ball lightning as charged eigenstate of elementary quaternion functions in real matrix form [5]. Its threshold surface field secures invariant size and total charge, with central potential as evolutionary parameter. Below magnetic field adds force-free electrodynamic solutions possibly relevant to silent decay of ball lightning as in an airborne event discussed by Kawano [6].

Newroth observed ball lightning formation on the windscreen of a small jet plane underway from Las Vegas to St. Paul, USA [7]. Flying between two storms the plane was racing to avoid bad weather. From his jump seat in the cockpit between two pilots he saw St. Elmo's fire playing on the inside of the windshield before him. Just as the pilots called the St. Elmo's fire very aggressive, sparks joined together into a perfect ball at face level straight ahead of him, the ball passed his head and disappeared through the door supporting his seat. Afterwards shaken pilots downplayed the event. Newroth's cockpit-born 'perfect ball' dovetails nicely with Jennison's 'perfect sphere' floating down the isle of a commercial airliner four decades earlier.

Let Cartesian co-ordinates in a 4-vector $\{w,\mathbf{x}\}$ with $\mathbf{x}=\{x,y,z\}$ span a quaternion space [5,9]. Combine $\Phi(w,\mathbf{x})$ as scalar potential of electric field $\mathbf{E}$ with $\mathbf{A}(w,\mathbf{x})$ as vector potential of magnetic field $\mathbf{B}$ into 4-vector $\{\Phi,\mathbf{A}\}$ for the potentials. Define 4×4 potential tensor $\mathbb{P}(w,\mathbf{x})$ in (1a) with $\mathbb{p}(w,\mathbf{x})$ in (1b) as its leading 3×3 minor through:

$$\mathbf{E} \equiv -\mathrm{grad}\Phi \quad ; \quad \mathbf{B} \equiv \mathrm{rot}\mathbf{A} \quad ; \quad -\mathrm{u} \equiv \mathrm{i}^2 \equiv \mathrm{j}^2 \equiv \mathrm{k}^2 \equiv \mathrm{i}\cdot\mathrm{j}\cdot\mathrm{k} \quad ; \quad \mathbb{P} \equiv \mathrm{u}\Phi + \mathrm{i}A_x + \mathrm{j}A_y + \mathrm{k}A_z \qquad (1a)$$

$$\mathbf{E} = \partial\mathbf{A}/\partial w \quad ; \quad \mathbf{B} = \mathbf{0} \quad ; \quad \mathbf{x}\times\mathbf{A} = \mathbf{0} \quad ; \quad \mathbb{p}\cdot\mathbf{x} = \mathbf{x}\,\partial\Phi/\partial w \qquad (1b)$$

with elementary matrices u,i,j,k from Appendix A extending complex calculus into quaternion space. By the regularity conditions in (1b) $\mathbf{B}=\mathbf{0}$ guarantees solutions without Lorentz forces, while $\mathbf{x}\times\mathbf{A}=\mathbf{0}$ aligns co-ordinate vector $\mathbf{x}$ with vector potential $\mathbf{A}$. Conditions (1b) also connect the potentials Φ and $\mathbf{A}$ via their w-derivatives, with $\partial\Phi/\partial w$ emerging as eigenvalue of minor tensor $\mathbb{p}$.

Accepted for presentation at VII International Conference "Atmosphere, Ionosphere, Safety" (AIS-2020), I. Kant University of Kaliningrad, postponed from June 07-13, 2020 by Covid-19 pandemic.

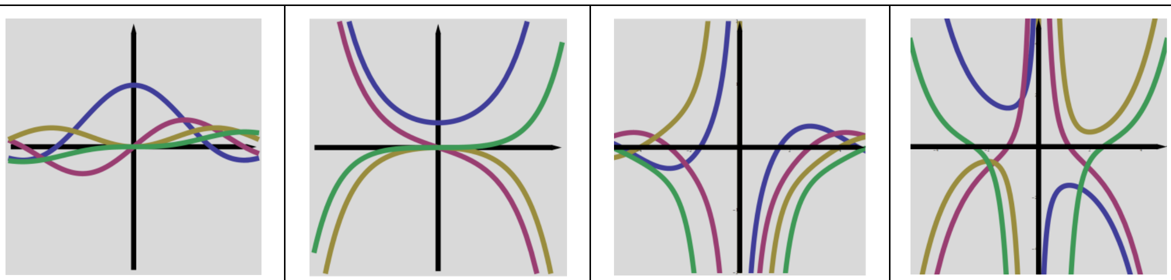

(a) Re[$j_n(w)$] (b) Im[$j_n(x)$] (c) Re[$y_n(w)$] (d) Im[$y_n(x)$]

Figure 2. Panels (a,b) plot real and imaginary parts of spherical Bessel functions j_n. Panels (c,d) likewise for modified versions y_n. The co-ordinate domains are $-3 \leqq w \leqq 3$. Blue, red, yellow, green labels orders n=0,1,2,3.

By quaternions space charge enters 3D solutions for atmospheric electricity [9]. Quaternion arctangens plots dipolar potential rings for thundercloud electrification. Meissner-type cusps in a ball plasma result from quaternion inversion. Swirling solutions from split-quaternions increase plasma stability by conservation of chirality [10]. Our quaternion model finds natural ball lightning deeply rooted in Hamiltonian dynamics [11].

MHD textbooks present a force-free solution for pinched plasma columns by Bessel functions [12,13]. Ball lightning as a force-free plasma sphere leads to complex Bessel functions of fractional order [4]. The explicit expressions for spherical Bessel functions j_n and modified versions y_n read:

$$j_n(\zeta) \equiv \alpha_n \sin(\zeta) - \beta_n \cos(\zeta) \quad ; \quad y_n(\zeta) \equiv \alpha_n \cos(\zeta) + \beta_n \sin(\zeta) \quad ; \quad \zeta \equiv w + \mathrm{i}\, x \tag{2a}$$

$$\alpha_0 = 1/\zeta \quad ; \quad \alpha_1 = 1/\zeta^2 \quad ; \quad \alpha_2 = 3/\zeta^3 - 1/\zeta \quad ; \quad \alpha_3 = 15/\zeta^4 - 6/\zeta^2 \tag{2b}$$

$$\beta_0 = 0 \quad ; \quad \beta_1 = -1/\zeta \quad ; \quad \beta_2 = -3/\zeta^2 \quad ; \quad \beta_3 = -15/\zeta^3 + 1/\zeta \tag{2c}$$

where (2b,c) lists amplitudes α_n and β_n for orders 0 to 3 as polynomials of $1/\zeta$. Notably j_n defines y_n by switching sine and cosine in (2a) with a change in sign, and vice versa. Panel (a) in Figure 2 shows pole-free profiles for real parts of j_n along the real w-axis, whereas such profiles for their imaginary parts in panel (b) diverge to infinity along the imaginary x-axis. For y_n in panels (c,d) all corresponding profiles cluster poles at the origin, and diverge to infinity along either co-ordinate axis. Underneath parametric plots in panels (a-d) of Figure 3 illustrate pole-freedom and divergences of j_n-sheets in the complex (w,x)-plane. For y_n dipolar singularities in panels (e-h) cluster sector-wise at the origin.

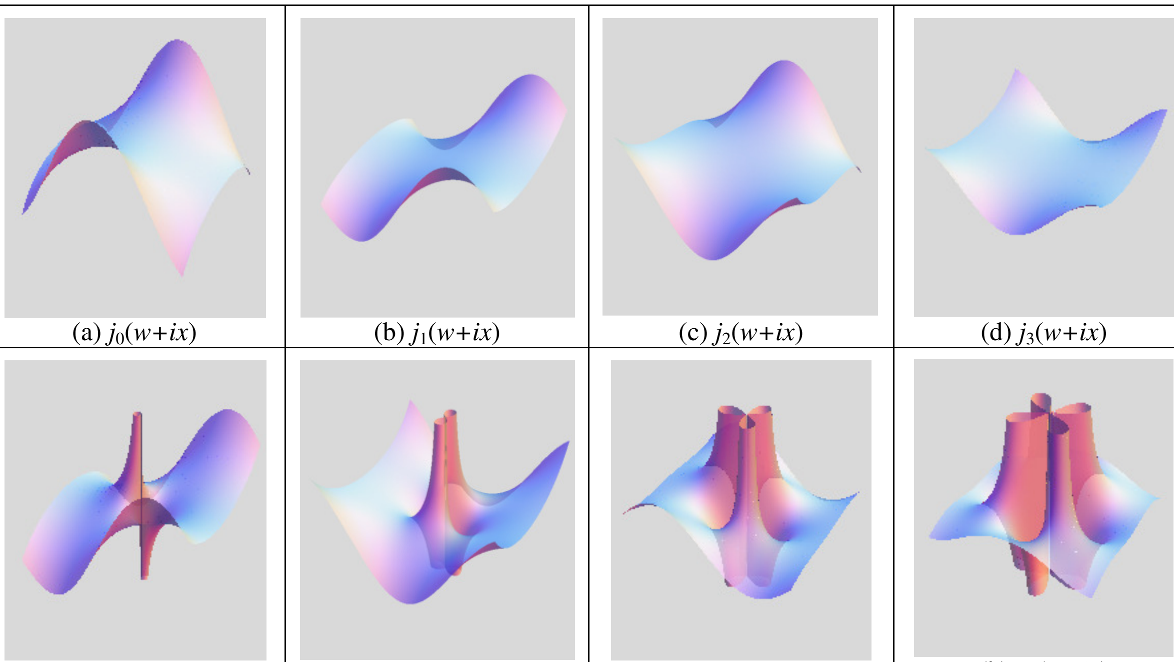

(a) $j_0(w+ix)$ (b) $j_1(w+ix)$ (c) $j_2(w+ix)$ (d) $j_3(w+ix)$

(e) $y_0(w+ix)$ (f) $y_1(w+ix)$ (g) $y_2(w+ix)$ (h) $y_3(w+ix)$

Figure 3. Panels (a,b,c,d) plot spherical Bessel functions j_0, j_1, j_2, j_3 in complex (w,x)-planes, and likewise for the modified versions y_0, y_1, y_2, y_3 in panels (e,f,g,h). Co-ordinate domain of w and x is $-3 \leqq w \leqq 3$ throughout.

Accepted for presentation at VII International Conference “Atmosphere, Ionosphere, Safety” (AIS-2020), I. Kant University of Kaliningrad, postponed from June 07-13, 2020 by Covid-19 pandemic.

Dassault Falcon 20 | Cockpit | Rear view

Figure 4. Aggressive St. Elmo's fire on central cockpit window triggered Newroth's ball lightning event

Pictures in Figure 4 detail a jet plane like the one carrying Newroth. On the flight and cockpit photos a central windshield window as formed his ball lightning is visible. Inside their plate glass usually a thin metallic layer serves for electric de-frosting and de-icing at high altitudes [6]. Boundary layer flow just outside the windscreen recalls our discharge nozzle tests for investigation of ball lightning [14].
For 3D plots we bring the leading modified Bessel function y_0=sin(w+ix)/(w+ix) in quaternion form. By the addition formulas for sine and cosine the 4-vector potentials Φ and **A** read:

$$\begin{aligned} &\{\Phi,\mathbf{A}\} = j_0 = \{aw, b\mathbf{x}\} && a = (-w\cos w\cosh r + r\sin w\sinh r)/(w^2+r^2) && r^2 \equiv \mathbf{x}\cdot\mathbf{x} \\ &\mathbf{A} \equiv \{A_x, A_y, A_z\} && b = (\;w\sin w\sinh r/r + \cos w\cosh r)/(w^2+r^2) && \mathbf{x} \equiv \{x,y,z\} \end{aligned} \qquad (4)$$

with hyperbolic functions sinh$r$≡½(e^r-e^{-r}) and cosh$r$≡½(e^r+e^{-r}) that blow up along imaginary axes in Figures 2 and 3. Remarkably the 3D zero-potential sheets at w=0 in Eq. 4 avoid infinities in panels a,b,c,d of Figure 5, and poles at the origin. Shape and smoothness qualify such sheets as precursors of ball lightning formation by St. Elmo's fire on flat dielectric surface as witnessed by Newroth.

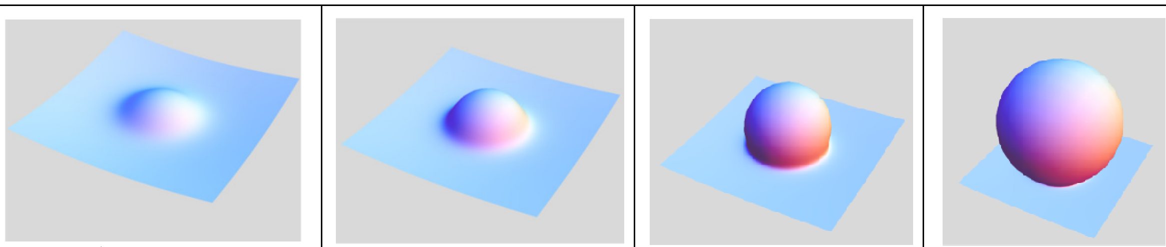

(a) **A**(w=0,x,y,z=1) | (b) **A**(w=0,x,y,z=0,7) | (c) **A**(w=0,x,y,z=0,4) | (d) **A**(w=0,x,y,z=0,4)

Figure 5. Panels (a,b,c,d) plot successive 3D zero-potential sheets via vector potential **A** as modified Bessel-function y_0 in quaternion form. Co-ordinates w,x,y,z are Cartesian. The domain for x and y is {−3,3}.

References

1 W. Lee, et al., *Synthetic electromagnetic knot in a three-dimensional skyrmion*, 2018, Sci. Adv. **4**.
2 A.F. Ranada, M. Soler and J.L. Trueba, *A model of ball lightning as a magnetic knot with linked steamers*. 1998, J. Geophys. Res., pp. 23.309-313.
3 B.M. Smirnov, *The properties and the nature of ball lighting*. 1987, Phys. Rep., **152**, pp. 177-226.
4 M. Abramowitz and I.A. Stegun, *Handbook of Mathematical Functions*. 1968, Dover Pubs., pp. 437-445.
5 G.C. Dijkhuis, *Ball lightning as thermodynamic limit of the Periodic System*. 2010, in: The Atmosphere and Ionosphere: Dynamics, Processes and Monitoring, Eds. V.L. Bychkov, G.V. Golubkov and A.I. Nikitin. Springer, pp. 349-354.
6 S. Kawano, *Proposal of how ball lightning emerges in fuselage and of how it gets electric energy*. 2017, Proceedings of 2nd International Symposium on Lightning and Storm-related Phenomena (ISL-SRP), Aurillac (Cantal, France).
7 M. Newroth, *Ball lightning in the cockpit of a small jet plane*. 2006, Posted on The Weird Science Page database of Ball Lightning Reports. http://www.amasci.com/weird/unusual/blll.html.
8 R.C. Jennison, *Ball lightning*. 1969, Nature, **224**, p. 895.
9 G.C. Dijkhuis, *On 3D potential field solutions for atmospheric charge distributions.* 2010, PIERS Online, **6**, pp. 300-306. piers.org/piersonline/piers.php?volume=6&number=4&page=300

Accepted for presentation at VII International Conference "Atmosphere, Ionosphere, Safety" (AIS-2020), I. Kant University of Kaliningrad, postponed from June 07-13, 2020 by Covid-19 pandemic.

10 Idem, *On ball lightning formation by soliton waves.* 2014, Proceedings of the 13th International Symposium on Ball Lightning, Zelenogradsk.
11 Idem, *On canonical eigenstates for ball lightning*. 2017, Proceedings of 2nd International Symposium on Ball Lightning and Storm-related Phenomena (ISL-SRP), Aurillac, France.
12 J.P. Freidberg, Ideal MHD. 2014, Cambridge University Press, p. 98.
13 P.H. Roberts, *An Introduction to Magnetohydrodynamics*. 1967, Longmans Green, London, p. 110.
14 G.C. Dijkhuis and J. Pijpelink, *Performance of high-voltage test facility designed for investigation of ball lightning*. 1989, in: *Science of Ball Lightning (Fireball)*. Ed. Y.-H. Ohtsuki, World Scientific, pp.325-337.
15 H.P. Robertson and T.W Noonan, *Relativity and Cosmology*. 1968, W.B. Saunders Company, p. 87.

Appendix A Quaternion form for force-free electromagnetic potentials

Relativistic theory combines electromagnetic fields **E**=$\{E_x,E_y,E_z\}$ and **B**=$\{B_x,B_y,B_z\}$ in a traceless 4×4 tensor form through [15]:

$$\mathbb{F} \equiv \begin{bmatrix} 0 & -E_x & -E_y & -E_z \\ E_x & 0 & B_z & -B_y \\ E_y & -B_z & 0 & B_x \\ E_z & B_y & -B_x & 0 \end{bmatrix}, \quad \mathbb{f} \equiv \begin{bmatrix} 0 & B_z & -B_y \\ -B_z & 0 & B_x \\ B_y & -B_x & 0 \end{bmatrix}, \quad \begin{matrix} \Delta\mathbb{F} = (\mathbf{E}\cdot\mathbf{B})^2 \\ \Delta\mathbb{f} = 0 \end{matrix} \tag{A1}$$

Field determinant $\Delta\mathbb{F}$ is positive or zero, and the magnetic entries in minor determinant $\Delta\mathbb{f}$ always cancel. Remarkably the anti-symmetric signature of field tensor $\mathbb{F}$ returns in regular quaternion form. Replace zeroes in $\mathbb{F}$ by scalar potential Φ, and likewise the vectors **E**,**B** in $\mathbb{F}$ by vector potential **A**=$\{A_x,A_y,A_z\}$. Then potential tensor $\mathbb{P}$ and minor tensor $\mathbb{p}$ result as:

$$\mathbb{P} \equiv \begin{bmatrix} \Phi & -A_x & -A_y & -A_z \\ A_x & \Phi & A_z & -A_y \\ A_y & -A_z & \Phi & A_x \\ A_z & A_y & -A_x & \Phi \end{bmatrix}, \quad \mathbb{p} \equiv \begin{bmatrix} \Phi & A_z & -A_y \\ -A_z & \Phi & A_x \\ A_y & -A_x & \Phi \end{bmatrix}, \quad \begin{matrix} \Delta\mathbb{P} = (\Phi^2 + \mathbf{A}\cdot\mathbf{A})^2 \\ \Delta\mathbb{p} = \Phi\sqrt{\Delta\mathbb{P}} \end{matrix} \tag{A2}$$

with **E**=−gradΦ and **B**=rot**A** as standard definitions of the electromagnetic fields. We find determinant $\Delta\mathbb{P}$ as positive or zero, and its minor $\mathbb{p}$ as a real number. Four partial derivatives of $\mathbb{P}$ define four 4×4 elementary matrices u,i,j,k in (A3a) that restore $\mathbb{P}$ to traditional quaternion form in (A3b) through:

$$\mathrm{u} \equiv \partial\mathbb{P}/\partial\Phi\ ,\quad \mathrm{i} \equiv \partial\mathbb{P}/\partial A_x\ ,\quad \mathrm{j} \equiv \partial\mathbb{P}/\partial A_y\ ,\quad \mathrm{k} \equiv \partial\mathbb{P}/\partial A_z \tag{A3a}$$

$$-\mathrm{u} = \mathrm{i}^2 = \mathrm{j}^2 = \mathrm{k}^2 = \mathrm{i}\cdot\mathrm{j}\cdot\mathrm{k}\ ,\quad \mathbb{P} = \mathrm{u}\Phi + \mathrm{i}A_x + \mathrm{j}A_y + \mathrm{k}A_z \tag{A3b}$$

with u as 4×4 unit matrix. In explicit and in vector form our twelve conditions for regularity read:

$$\begin{matrix} \partial_x\Phi = -\partial_w A_x & \partial_y A_z = \partial_z A_y & yA_z = zA_y & x\partial_w\Phi = x\partial_x A_x + y\partial_y A_x + z\partial_z A_x \\ \partial_y\Phi = -\partial_w A_y & \partial_z A_x = \partial_x A_z & zA_x = xA_z & y\partial_w\Phi = x\partial_x A_y + y\partial_y A_y + z\partial_z A_y \\ \partial_z\Phi = -\partial_w A_z & \partial_x A_y = \partial_y A_x & xA_y = yA_x & z\partial_w\Phi = x\partial_x A_z + y\partial_y A_z + z\partial_z A_z \\ \mathbf{E} = \partial\mathbf{A}/\partial w & \mathbf{B} = \mathbf{0} & \mathbf{x}\times\mathbf{A} = \mathbf{0} & \mathbb{p}\cdot\mathbf{x} = \mathbf{x}\,\partial\Phi/\partial w \end{matrix} \tag{A4}$$

ensuring 3D force free electromagnetic solutions by extension of any complex functions. A well-known analogy links electromagnetics as above with 3D vortex flow in incompressible inviscid fluids.